

1 **Improving hydrological projection performance under contrasting**
2 **climatic conditions using spatial coherence through a hierarchical**
3 **Bayesian regression framework**

4 **Zhengke Pan^{a,b}, Pan Liu^{a,b,*}, Shida Gao^{a,b}, Jun Xia^{a,b,c}, Jie Chen^{a,b}, Lei Cheng^{a,b},**

5

6 ^aState Key Laboratory of Water Resources and Hydropower Engineering Science, Wuhan
7 University, Wuhan 430072, China

8

9 ^bHubei Provincial Collaborative Innovation Center for Water Resources Security, Wuhan
10 430072, China

11 ^cChinese Academy of Sciences, Beijing 100864, China

12

13 *Corresponding author. Email: liupan@whu.edu.cn; Tel: +86-27-68775788; Fax:
14 +86-27-68773568

15

16

17

18

19 **ABSTRACT**

20 Understanding the projection performance of hydrological models under contrasting
21 climatic conditions supports robust decision making, which highlights the need to
22 adopt time-varying parameters in hydrological modeling to reduce the performance
23 degradation. Many existing literatures model the time-varying parameters as functions
24 of physically-based covariates; however, a major challenge remains in finding
25 effective information to control the large uncertainties that are linked to the additional
26 parameters within the functions. This paper formulated the time-varying parameters
27 for a lumped hydrological model as explicit functions of temporal covariates and used
28 a hierarchical Bayesian (HB) framework to incorporate the spatial coherence of
29 adjacent catchments to improve the robustness of the projection performance. Four
30 modeling scenarios with different spatial coherence schemes, and one scenario with a
31 stationary scheme for model parameters, were used to explore the transferability of
32 hydrological models under contrasting climatic conditions. Three spatially adjacent
33 catchments in southeast Australia were selected as case studies to examine validity of
34 the proposed method. Results showed that (1) the time-varying function improved the
35 model performance but also amplified the projection uncertainty compared with
36 stationary setting of model parameters; (2) the proposed HB method successfully
37 reduced the projection uncertainty and improved the robustness of model performance;
38 and (3) model parameters calibrated over dry periods were not suitable for predicting
39 runoff over wet periods because of a large degradation in projection performance.
40 This study improves our understanding of the spatial coherence of time-varying
41 parameters, which will help improve the projection performance under differing
42 climatic conditions.

43 **Keywords:** Climate change; Hierarchical Bayesian; Hydrological model parameters;
44 Spatial coherence; Streamflow projection; Contrasting climatic conditions

45

46

47 **1. INTRODUCTION**

48 Long-term streamflow projection is an important part of effective water
49 resources planning because it can predict future scarcity in water supply and help
50 prevent floods. Streamflow projections typically involve the following: (i) calibrating
51 hydrological model parameters with partial historical observations (e.g., precipitation,
52 evaporation and streamflow); (ii) projecting streamflow under periods that are outside
53 of those for model calibration; and (iii) evaluating the model projection performance
54 with certain criteria. One of the most basic assumptions of this process—that the
55 calibrated model parameters are stationary and can be applied to predict catchment
56 behaviors in the near future, has been widely questioned (Brigode et al., 2013;
57 Broderick et al., 2016; Chiew et al., 2014; Chiew et al., 2009; Ciais et al., 2005;
58 Clarke, 2007; Cook et al., 2004; Coron et al., 2012; Deng et al., 2016; Merz et al.,
59 2011; Moore and Wondzell, 2005; Moradkhani et al., 2005, 2012; Pathiraja et al.,
60 2016, 2018; Patil and Stieglitz, 2015; Westra et al., 2014; Xiong et al., 2019; Zhang et
61 al., 2018).

62 Many previous studies have explored the transferability of stationary parameters
63 to periods with different climatic conditions. They have concluded that hydrological
64 model parameters are sensitive to the climatic conditions of the calibration period
65 (Chiew et al., 2009, 2014; Coron et al., 2012; Merz et al., 2011; Renard et al., 2011;
66 Seiller et al., 2012; Vaze et al., 2010). For instance, Merz et al. (2011) calibrated
67 model parameters using six consecutive 5-year periods between 1976 and 2006 for

68 273 catchments in Austria and found that the calibrated parameters representing snow
69 and soil moisture processes showed significant trend in the study area. Other studies
70 have found that degradation in model performance was directly related to the
71 difference in precipitation between calibration and verification periods (Coron et al.,
72 2012; Vaze et al., 2010). One proposal for managing this problem is to calibrate
73 model parameters in periods with similar climatic conditions to the near future, but
74 future streamflow observations are unavailable. Thus, it is still necessary to reduce the
75 magnitude of performance loss and improve the robustness of the projection
76 performance using calibrated parameters based on the historical records, even though
77 the climatic conditions in the future may be dissimilar to those used for model
78 calibration.

79 Several recent studies have found that hydrological models with time-varying
80 parameters exhibited a significant improvement in its projection performance
81 compared with the stationary parameters (Deng et al., 2016, 2018; Westra et al., 2014).
82 The functional method is one of the most promising ways to model time-varying
83 parameters and shows its excellence in improving the model projection performance
84 (Guo et al., 2017; Westra et al., 2014; Wright et al., 2015). This method models the
85 time-varying parameter(s) as function(s) of physically-based covariates (e.g.,
86 temporal covariate and Normalized Difference Vegetation Index). Generally, the
87 hydrological model is run with various assumed functions, the best functional forms
88 of time-varying parameters can be obtained by comparing the evaluation criteria.

89 However, a major challenge for the application of the functional method remains in
90 finding effective information to control the large uncertainties that are linked to the
91 additional parameters describing these regression functions.

92 Similarity of adjacent catchments has been verified its validity in controlling the
93 estimation uncertainty of model parameters (Bracken et al., 2018; Cha et al., 2016;
94 Cooley et al., 2007; Lima and Lall, 2009; Najafi and Moradkhani, 2014; Sun and Lall,
95 2015; Sun et al., 2015; Yan and Moradkhani, 2015). The level of similarity of
96 different catchments is known as spatial coherence. For instance, Sun and Lall (2015)
97 used the spatial coherence of trends in annual maximum precipitation in the United
98 States, and successfully reduced the parameter estimation uncertainty in their at-site
99 frequency analysis. In general, there are three methods to consider the spatial
100 coherence between different catchments in parameter estimation. The first one is no
101 pooling, which means every catchment is modeled independently, and all parameters
102 are catchment-specific. The second one is complete pooling, which means all
103 parameters are considered to be common across all catchments. The third/last one is
104 hierarchical Bayesian (HB) framework, also known as partial pooling, which means
105 some parameters are allowed to vary by catchments and some parameters are assumed
106 to be drawn from a common hyper-distribution across the region that consists of
107 different catchments. In these three approaches, the HB framework has been proved
108 as the most efficient method to incorporate the spatial coherence to reduce the
109 estimation uncertainty because it has the advantage of shrinking the local parameter

110 toward the common regional mean and including an estimation of its variance or
111 covariance across the catchments (Bracken et al., 2018; Sun and Lall, 2015; Sun et al.,
112 2015). In the field of hydrological modeling, most proceeding literatures were focused
113 on no pooling models that neglect the spatial coherence between catchments
114 (Heuvelmans et al., 2006; Lebecherel et al., 2016; Merz and Blöschl, 2004; Oudin et
115 al., 2008; Singh et al., 2012; Tegegne and Kim, 2018; Xu et al., 2018); little attention
116 has been paid to the HB framework. Thus, we want to fill this gap and explore the
117 applicability of the spatial coherence through the HB framework in hydrological
118 modeling with the time-varying parameters.

119 The objectives of this paper were to: (1) verify the effect of the time-varying
120 model parameter scheme on model projection performance and uncertainty analysis
121 compared with stationary model parameters; (2) verify the projection performance of
122 considering spatial coherence of adjacent catchments through the HB framework
123 compared with spatial incoherence; and (3) compare the model projection
124 performance for different climatic transfer schemes.

125 The rest of the paper is organized as follows. Section 2 outlines the methodology
126 employed in this study including differential split sample test (DSST) for segmenting
127 the historical series, the hydrological model, and the two-level HB framework for
128 incorporating spatial coherence from adjacent catchments. Section 3 presents the
129 information on the study area and data. The results and discussion are described in
130 section 4. Section 5 summarizes the main conclusions of the study.

131 **2. METHODOLOGY**

132 The methodology is outlined by a flowchart in Figure 1, and is summarized as
133 follows:

134 (1) A temporal parameter transfer scheme is implemented (described in section
135 2.1) using a classic DSST procedure in which the available data are divided into
136 non-dry and dry periods;

137 (2) A daily conceptual rainfall-runoff model is used (outlined in section 2.2);

138 (3) A two-level HB framework is used to incorporate spatial coherence in
139 hydrological modeling (described in section 2.3). The process layer (first level) of the
140 framework models the temporal variation in the model parameters using a
141 time-varying function, while the prior layer (second level) models the spatial
142 coherence of the regression parameters in the time-varying function. Four modeling
143 scenarios with different spatial coherence schemes, and one scenario with a stationary
144 scheme for the model parameter, are used to evaluate the transferability of
145 hydrological models under contrasting climatic conditions;

146 (4) Likelihood function and parameter estimation methods are applied (outlined
147 in section 2.4); and

148 (5) The criteria are used to evaluate the model performance for various model
149 scenarios (described in section 2.5).

150 **2.1 Differential split sampling test**

151 To verify the projection performance of the rainfall-runoff model under
152 contrasting climatic conditions (non-dry and dry periods), a classic DSST using
153 annual rainfall records was adopted.

154 Two separate tasks were needed to develop the DSST method into a working
155 system. The first step was to define the “dry period”. The method to define the dry
156 period is adopted from Saft et al. (2015), which is a rigorous identification method
157 that treats autocorrelation in the regression residuals, undertakes global significance
158 testing, and defines the start and end of the droughts individually for each catchment.
159 Saft et al. (2015) tested several algorithms for dry period delineation, which
160 considered different combinations of dry run length, dry run anomaly and various
161 boundary criteria, and found that the identification results of dry period by one of the
162 algorithms showed marginal dependence on the algorithm and the main results were
163 robust to different algorithms. The detailed processes could be found on Saft et al.
164 (2015) and also are generalized as follows.

165 Firstly, the annual rainfall data were calculated relative to the annual mean, and
166 the anomaly series was divided by the mean annual rainfall and smoothed with a 3
167 year moving window. Secondly, the first year of the drought remained the start of the
168 first 3 year negative anomaly period. Thirdly, the exact end date of the dry period was
169 determined through analysis of the unsmoothed anomaly data from the last negative 3
170 year anomaly. The end year was identified as the last year of this 3 year period unless:

171 (i) there was a year with a positive anomaly $>15\%$ of the mean, in which case the end
172 year is set to the year prior to that year; or (ii) if the last two years have slightly
173 positive anomalies (but each $<15\%$ of the mean), in which case the end year is set to
174 the first year of positive anomaly; (iii) to ensure that the dry periods are sufficiently
175 long and severe, in the subsequent analysis, the authors use dry periods with the
176 following characteristics: length ≥ 7 years; mean dry period anomaly $<25\%$.

177 In the second step, the non-dry period was defined as the complement of the dry
178 period in the historical records. A similar approach to define the dry and non-dry
179 periods was used by Fowler et al. (2016).

180 In the DSST method, the model parameters calibrated in the non-dry period were
181 evaluated in the dry period, and vice versa. In addition, criteria, i.e. NSE_{sqrt} , BIAS and
182 DIC illustrated in the section 2.5, were used to evaluate the performance of the
183 calibrated parameters for different transfer schemes.

184 **2.2 The rainfall-runoff model**

185 The hydrological model used in this study is the GR4J (modèle du Génie Rural à
186 4 paramètres Journalier), which is a lumped conceptual rainfall-runoff model (Perrin
187 et al., 2003). The original version of the GR4J model (Figure 2) comprised four
188 parameters (Perrin et al., 2003): production store capacity (θ_1 mm), groundwater
189 exchange coefficient (θ_2 mm), 1-day-ahead maximum capacity of the routing store
190 (θ_3 mm), and the time base of the unit hydrograph (θ_4 days). More details on the
191 GR4J model can be found in Perrin et al. (2003).

192 The GR4J model is a parsimonious, but efficient model. The model has been
193 used successfully across a wide range of hydro-climatic conditions across the world,
194 including the crash testing of model performance under contrasting climatic
195 conditions (Coron et al., 2012), and the simulation of runoff for revisiting the
196 deficiency in insufficient model calibration (Fowler et al., 2016). In addition, Fowler
197 et al. (2016) verified that conceptual rainfall-runoff models were more capable under
198 changing climatic conditions than previously thought. These characteristics make the
199 GR4J particularly suitable as a starting point for implementing modifications and/or
200 improving predictive ability under changing climatic conditions.

201 **2.3 The HB framework for the time-varying model parameter**

202 In this study, various versions were constructed for evaluating the projection
203 capabilities of models for contrasting climatic conditions (non-dry and dry periods),
204 and for considering the temporal variation and spatial coherence of parameter θ_1 .

205 2.3.1 Process layer: temporal variation of the model parameter

206 As described in the literature (Perrin et al., 2003; Renard et al., 2011; Westra
207 et al., 2014), the parameter θ_1 , which represents the primary storage of water in
208 the catchment, is the most sensitive parameter in the GR4J model structure, and
209 stochastic variations of this parameter have the largest impact on model projection
210 performance (Renard et al., 2011; Westra et al., 2014). In addition, the temporal
211 variation in the catchment storage capacity was physically interpretable. Periodic

212 variations in the production store capacity θ_1 can be induced by the periodicity in
213 precipitation and in seasonal vegetation growth and senescence. In the present
214 study, θ_1 was constructed to account for the periodical variation that had a
215 significant impact on the extensionality of the model. The periodical variation in
216 catchment storage capacity θ_1 is described by a sine function, using amplitude and
217 frequency.

218 Thus, for any catchment c , the full temporal regression function for θ_1 at the
219 process layer is:

220 Process layer:
$$\theta_1(c, t) = \alpha(c) + \beta(c) \sin[\omega(c)t] \quad (1)$$

221 where α , β , ω are regression parameters for the specific DSST method, and α
222 signifies the intercept, and $\{\beta, \omega\}$ represents the amplitude and frequency of the
223 sine function, respectively. The t is the time step. If model parameter θ_1 is constant
224 then $\alpha=\beta=\omega=0$ suffices in Eq.1 and the resulting model simplifies to a stationary
225 hydrological model.

226 2.3.2 Prior layer: spatial coherence of regression parameters

227 For a heterogeneous region that is distinctly non-uniform in climatic and
228 geologic conditions, different catchments within the region typically have different
229 catchment storage capacities and different values of production store capacity θ_1 . For
230 a homogeneous region prescribed by similar climatic and geologic conditions in each
231 part, the production store capacity (in Eq. 1) is expected to be the same among

232 different catchments of the region. The model could be improved by considering
233 spatial input, i.e., the spatial coherence of parameters across adjacent catchments
234 (Chen et al., 2014; Lima et al., 2016; Merz and Blöschl, 2004; Oudin et al., 2008;
235 Patil and Stieglitz, 2015; Renard et al., 2011; Sun et al., 2014).

236 In this study, independent Gaussian prior distributions were used for the
237 regression parameters $\{\beta, \omega\}$ at the prior layer to include the potential spatial
238 coherence. Their equations are as follows:

239 Prior layer:
$$\begin{aligned}\beta(c) &= N(\mu_2, \sigma_2^2) \\ \omega(c) &= N(\mu_3, \sigma_3^2)\end{aligned}\tag{2}$$

240 where μ_2, μ_3, σ_2 and σ_3 are hyper-parameters, and $N(\cdot)$ represents the
241 hyper-distribution, i.e., a Gaussian distribution. Independent Gaussian distributions
242 were assumed for the regression parameters $\{\beta, \omega\}$ that were used to model spatial
243 coherence based on practical considerations. The prior layer of the HB framework
244 aims to describe the variation of $\{\beta, \omega\}$ in space by means of a Gaussian spatial
245 process in which the mean value depends on covariates describing regional
246 characteristics. Regression parameters β and ω are the most important
247 parameters in the regression function and can reflect the spatial connection of
248 variation and cyclicity of catchment production storage capacity among catchments.
249 A similar setting was made in Sun and Lall (2015) and Sun et al. (2015).

250 2.3.3 Modeling scenarios

251 Five modeling scenarios (Table 1) were carried out to assess the effect of spatial
252 coherence on the time-varying function. Different levels of spatial coherence of
253 $\{\beta, \omega\}$ were assumed in scenarios 1 to 4, while in scenario 5 parameter θ_1 was set
254 to be constant to provide a comparison. It should be noted that the estimates for
255 spatially coherent regression parameters would be shared by different catchments
256 while other quantities would be regarded as catchment-specific variables. For
257 example, regression parameter β is spatially linked in scenario 1, i.e., $\beta(c) =$
258 $N(\mu_2, \sigma_2^2)$, which means that the estimates of β are shared by all catchments.
259 Meanwhile, regression parameters ω_{1-1} , ω_{1-2} , and ω_{1-3} are used as independent
260 variables to represent the frequency of model parameter θ_1 in different catchments.
261 The number of unknown quantities in different scenarios are as follows: fifteen in
262 scenarios 1 and 2, thirteen in scenario 3 and eighteen in scenario 4. The prior ranges
263 of all unknown quantities in different scenarios and both DSST schemes could be
264 found in Table S1 in Supplement material.

265 **2.4 Estimation and projection**

266 The objective function and parameter inference methods were used to derive the
267 posterior distribution of all unknown quantities, as illustrated below.

268 2.4.1 Objective function

269 For a specific catchment, the model parameters were calibrated to minimize the
270 following objective function, which was adopted from Coron et al. (2012).

$$271 \quad \varepsilon_c [\theta_1, \theta_2, \theta_3, \theta_4] = -RMSE[\sqrt{Q}](1 + |1 + BIAS|) \quad (3)$$

272 where

$$273 \quad RMSE[\sqrt{Q}] = \sqrt{\frac{1}{T} \sum_{t=1}^T [Q_{sim}(t) - Q_{obs}(t)]^2} \quad (4)$$

274 and $RMSE[\sqrt{Q}]$ refers to the root-mean-square error, in which Q_{sim} is derived by
275 the adopted hydrological model.

276 Coron et al. (2012) showed that this objective function performed well. In this
277 function, the combination of $RMSE[\sqrt{Q}]$ and $BIAS$ (Eq.7) gives weight to dynamic
278 representation as well as the water balance. Using square-root-transformed flows to
279 compute the RMSE reduces the influence of high flows during the calibration period
280 and provides a good compromise between alternative criteria.

281 In the case of multiple catchments, the objective function of the HB framework
282 was the product of Eq.3 and the conditional probability of spatial coherence of
283 regression parameters f_N . It was written as follows:

$$\text{Scenario 1: } \Lambda = \prod_{c=1}^C \varepsilon_c \left[\theta_1(t, c), \theta_2(c), \theta_3(c), \theta_4(c) | \alpha(c), \beta, \omega(c) \right] \bullet f_N(\beta | \mu_2, \sigma_2)$$

$$\text{Scenario 2: } \Lambda = \prod_{c=1}^C \varepsilon_c \left[\theta_1(t, c), \theta_2(c), \theta_3(c), \theta_4(c) | \alpha(c), \beta(c), \omega \right] \bullet f_N(\omega | \mu_3, \sigma_3)$$

$$284 \quad \text{Scenario 3: } \Lambda = \prod_{c=1}^C \varepsilon_c \left[\theta_1(t, c), \theta_2(c), \theta_3(c), \theta_4(c) | \alpha(c), \beta, \omega \right] \bullet \prod_{n=1}^2 f_N(\beta, \omega | \mu_2, \sigma_2, \mu_3, \sigma_3) \quad (5)$$

$$\text{Scenario 4: } \Lambda = \prod_{c=1}^C \varepsilon_c \left[\theta_1(t, c), \theta_2(c), \theta_3(c), \theta_4(c) \right]$$

$$\text{Scenario 5: } \Lambda = \prod_{c=1}^C \varepsilon_c \left[\theta_1(c), \theta_2(c), \theta_3(c), \theta_4(c) \right]$$

285 where the number of catchments in the region is represented by C , and the Gaussian
 286 spatial function between regression parameters β, ω and hyper-parameters μ_2 ,
 287 μ_3 , σ_2 and σ_3 are denoted by $f_N()$. N refers to the Gaussian distribution and
 288 n represents the number of regression parameters that are spatially coherent. The
 289 Gaussian distribution is one of the widely used distributions for describing the prior
 290 layer within the HB framework and has been applied in many previous studies, such
 291 as Sun et al (2015, 2016) and Chen et al (2014).

292 2.4.2 Inference

293 The likelihood functions defined in Eqs. 3 and 5 pose a computational challenge
 294 because their dimensionality grows (primarily related to the number of
 295 catchment-specific parameters) with the number of catchments considered. The
 296 unknown parameters, including model parameters (θ_2 , θ_3 , and θ_4), regression
 297 parameters α , β and ω (if present), and hyper-parameters μ_2 , σ_2 , μ_3 and
 298 σ_3 , are sampled and estimated simultaneously using the Shuffled Complex Evolution
 299 Metropolis (SCEM-UA) sampling method (Ajami et al., 2007; Vrugt et al., 2003,
 300 2009). The SCEM-UA sampling method is a widely used Markov Chain Monte Carlo

301 algorithm for simulating the posterior probability distribution of parameters that are
302 conditional on the current choice of parameters and data. When compared with
303 traditional Metropolis-Hasting samplers, the SCEM-UA algorithm more efficiently
304 reduces the number of model simulations needed to infer the posterior distribution of
305 parameters, (Ajami et al., 2007; Duan et al., 2007; Liu et al., 2014; Liu and Gupta,
306 2007; Vrugt et al., 2003). Convergence is assessed by evolving three parallel chains
307 with 30000 random samples, the posterior distributions of parameters are evaluated by
308 the Gelman-Rubin convergence value and are confirmed that the convergence value is
309 smaller than the threshold 1.2 (Gelman et al., 2013). In addition, the uniform
310 distribution is used as the prior distribution for all unknown quantities. Because that
311 the prior distribution has no impact on final evaluation of different scenarios, the prior
312 distributions are not presented in Eq.5.

313 **2.5 Model performance criteria**

314 Three criteria were used to assess the projection performance during the
315 verification periods.

316 (1) The first criterion was NSE_{sqrt} , known as the arithmetic square root of
317 Nash-Sutcliffe Efficiency (Coron et al., 2012; Moriasi et al., 2007; Nash and Sutcliffe,
318 1970). When compared with the classic NSE, NSE_{sqrt} gives an intermediate, more
319 balanced picture of the overall hydrograph fit because it can reduce the influence of
320 high flow. It is expressed as:

321
$$NSE_{sqr} = 1 - \frac{\sum_{t=1}^T [\sqrt{Q_{obs}(t)} - \sqrt{Q_{sim}(t)}]^2}{\sum_{t=1}^T [\sqrt{Q_{obs}(t)} - \sqrt{\bar{Q}_{obs}}]^2} \quad (6)$$

322 where $Q_{sim}(t)$ and $Q_{obs}(t)$ represent the simulated and observed daily streamflow
 323 values for the t^{th} day, respectively; \bar{Q}_{obs} is the mean of the observed daily
 324 streamflow for the calculation interval; and T refers to the length of the calculation
 325 period.

326 (2) The second criterion is the BIAS, which is a part of the objective function
 327 Eq.3.

328
$$BIAS = \frac{\sum_{t=1}^T [Q_{sim}(t) - Q_{obs}(t)]}{\sum_{t=1}^T [Q_{obs}(t)]} \quad (7)$$

329 (3) The third criterion is the Deviance information criterion (DIC), which was
 330 defined by Spiegelhalter et al. (2002). It is a widely used and popular measure
 331 designed for Bayesian model comparison and is a Bayesian alternative to the standard
 332 Akaike Information Criterion. The DIC value for a Bayesian scenario is obtained as:

333
$$DIC = -2 \log(p(q|\theta_{Bayes}, \xi)) + 2p_{DIC} \quad (8)$$

334 where p_{DIC} is the effective number of parameters, defined as

335
$$p_{DIC} = 2 \left(\log(p(q|\theta_{Bayes}, \xi)) - \frac{1}{S} \sum_{s=1}^S \log(p(q|\theta^s, \xi)) \right) \quad (9)$$

336 where posterior mean $\theta_{Bayes} = \text{Expect}(\theta|q, \xi)$ and $s=1, \dots, S$, means the sequence
337 number of the simulated parameter set θ^s by the adopted SCEM-UA algorithm.
338 According to Spiegelhalter et al. (2002), scenarios with smaller DIC would be
339 preferred to scenarios with larger DIC.

340 (4) The fourth and fifth criteria are the Mean annual maximum flow (MaxF,
341 mm/d) and Mean annual minimum flow (MinF, mm/d), which are used to qualify the
342 performance of the high flows and low flows. These criteria are self-explanatory and
343 have been used in many studies to assess the magnitude of maximum and minimum
344 levels of flows (Ekstrom et al., 2018).

345 **3. Study area and data**

346 To evaluate the model performance, we used daily precipitation (mm/day),
347 evapotranspiration (mm/day), and streamflow (mm/day) time series records for three
348 unregulated and unimpaired catchments in south-eastern Australia, taken from the
349 national dataset of Australia (Zhang et al., 2013), covering 1976–2011. The streams
350 were unregulated: they were not subject to dam or reservoir regulations, which can
351 reduce the impact of human activity. The observed streamflow record contained at
352 least 11835 daily observations (equivalent to a record integrity of greater than 90%)
353 for 1976–2011, with acceptable data quality. The first complete year of data was used
354 for model warm-up to reduce the impact of the initial soil moisture conditions during
355 the calibration period.

356 The attributes of the south-eastern Australian catchments are shown in Table 2
357 and Figure 3. The IDs of these catchments are 225219 (Glencairn station on the
358 Macalister River: mean annual rainfall, potential evapotranspiration, and runoff are
359 1064 mm, 1142 mm, and 350 mm, respectively), 405219 (Dohertys station on the
360 Goulburn river: mean annual rainfall, potential evapotranspiration, and runoff are
361 1169 mm, 1193 mm, and 422 mm, respectively), and 405264 (D/S of Frenchman Ck
362 Jun station on the Big river: mean annual rainfall, potential evapotranspiration, and
363 runoff are 1406 mm, 1157 mm, and 469 mm, respectively). As shown in Figure 3,
364 these catchments are adjacent to each other. All catchments experienced a severe
365 multiyear drought around the end of the millennium. Saft et al. (2015) identified that
366 the rainfall-runoff relationship in these catchments was altered during the long-term
367 drought.

368 **4. Results and discussion**

369 Results from the DSST were used to assess the model projection performance for
370 five scenarios under contrasting climatic conditions. First, a DSST was conducted in
371 each catchment to divide original records into non-dry and dry periods. Then, the
372 projection performance for the five scenarios and associated parameter uncertainties
373 were evaluated using the criteria described above.

374 **4.1 Dry period identification**

375 As illustrated in Table 3 and Figure 4, the drought definition method identified
376 that the three catchments had similar dry period characteristics, with the same drought

377 start (1997) and end (2009) points. The mean dry period anomaly was less severe in
378 the Macalister catchment (225219), with a 6.95% reduction in the mean dry period
379 anomaly while the other two catchments experienced reductions of 9.84% (405219)
380 and 9.62% (405264).

381 In terms of changes in rainfall, both catchments had a reduction from the non-dry
382 to the dry periods of 11% on average, which was within the range that Vaze et al.
383 (2010) recommended for acceptable model simulations. Vaze et al. (2010) tested four
384 conceptual rainfall-runoff models in 61 catchments in southeast Australia using the
385 stationary scheme of model parameters, and found that the calibrated parameter sets
386 generally gave acceptable simulations provided rainfall changes were not too large
387 (no more than 15% dryer or 20% wetter than rainfall in the calibration period).

388 **4.2 Model performance in five scenarios**

389 As shown in Figures 5(a), 6(a) and 7, the calibrated model parameters yielded
390 good simulation performance over the calibrated periods for all criteria. For example,
391 the mean $NSE_{\text{sqr}}t$ score during the calibration period across these catchments remained
392 close to about 0.7 or slightly higher, regardless of which scenario was chosen.
393 However, when the same parameter sets were verified by simulating streamflow over
394 drier or wetter periods, the model performance was degraded, including both the
395 robustness and accuracy of projection performance. Furthermore, the magnitude of
396 performance loss increases along with the variation between the calibration and
397 verification periods.

398 Figure 5 shows the NSE_{sqrt} performance for calibration in a non-dry period and
399 verification in a dry period for each scenario in all catchments. All scenarios
400 performed well in all catchments with the mean NSE_{sqrt} reaching 0.81 during the
401 non-dry calibration period, and then all scenarios experienced a slight decrease in
402 performance ($NSE_{\text{sqrt}} = 0.75$) during the dry verification period. Scenario 4
403 (time-varying parameters without spatial inputs) and scenario 5 (temporally stable
404 parameters) generally performed better during the calibration period than the
405 scenarios that considered different levels of spatial coherence for the regression
406 parameters. During the verification period, the NSE_{sqrt} rank order changed (Figure 5b).
407 Scenario 4 had a higher median NSE_{sqrt} performance than scenario 5 in catchments
408 225219 and 405264, and was slightly inferior than the latter in catchment 405219,
409 which indicates the validity of the time-varying scheme for improving the model
410 performance. However, the introduction of additional regression parameters
411 (α, β and ω) at the same time amplified the model projection uncertainty in two of
412 three catchments (225219 and 405264). Fortunately, the appropriate adoption of
413 spatial coherence alleviates this problem. In the DSST scheme of calibrating in the
414 non-dry period and verifying in the dry period, scenario 3 exhibited the smallest
415 fluctuation range of NSE_{sqrt} estimate for all catchments, showed the highest median
416 value in catchment 225219, and was the second best scenario in the other two
417 catchments (405219 and 405264) during the verification period. The highest median
418 NSE_{sqrt} performance in scenarios 4 and 5 during the calibration period did not
419 guarantee the same superior performance during the verification period. This

420 illustrates the deficiency of time-varying and stationary schemes of model parameters
421 when spatial inputs from adjacent catchments are not considered.

422 Similarly, Figure 6 illustrates the NSE_{sqrt} performance for each scenario in all
423 catchments for calibration in the dry period and verification in the non-dry period. All
424 scenarios performed well for all catchments with the mean NSE_{sqrt} reaching 0.75 in
425 the dry calibration period and 0.79 in the non-dry verification period. As shown in
426 Figure 5, models experienced a slight improvement in NSE_{sqrt} performance when
427 transferred from the dry period to the non-dry period. However, the projection
428 performance calibrated using a contrasting climatic condition was inferior to the
429 simulation performance that was directly calibrated from the climatic condition,
430 compared with Figures 5(a) and 6(b), or Figure 6(a) and 5(b). For example, the
431 NSE_{sqrt} performance in Figure 6(b) is inferior to that in Figure 5(a). By comparing
432 scenarios in the calibration period, it was found that scenarios 4 and 5 exhibited the
433 highest performance in two of three catchments (405219 and 405264), followed
434 successively by scenario 3, scenario 2, and scenario 1. During the verification period,
435 the median NSE_{sqrt} performance in scenario 4 was 0.80% higher than scenario 5,
436 however, the variation range in scenario 4 was 53% wider than the latter. In the DSST
437 scheme of calibrating in the dry period and verifying in the non-dry period, scenario 3,
438 which considered both spatial coherence of regression parameters β and ω
439 between different catchments, exhibited the highest median NSE_{sqrt} for all catchments,
440 had the smallest fluctuation range in two catchments (405219 and 405264) and is the

441 second smallest scenario in catchment 22519 during the verification period. These
442 results demonstrate that the time-varying scheme for model parameters improved the
443 median $NSE_{\text{sqr}}t$ performance but also amplified the projection uncertainty compared
444 with the results from the stationary scheme for model parameters. Compared with
445 other model scenarios, the incorporation of spatial coherence of both regression
446 parameters in scenario 3 reduced the projection uncertainty and improved the
447 robustness of the model performance, with the smallest fluctuation ranges in most
448 options under the contrasting climatic conditions. It indicates that the spatial setting of
449 model parameters between different catchments provided a clear input for reducing
450 the uncertainty of the model projection performance during the verification period. In
451 addition, it also should be noted that model parameters calibrated over dry periods,
452 contrastively, were not suitable for predicting runoff over wet periods because of a
453 larger degradation in projection performance than the scheme with the adverse
454 calibration-verification direction.

455 Comparing the DIC results for both DSST schemes in Table 4 and Table 5, the
456 best DIC value is achieved by scenario 3, which incorporates the spatial coherence of
457 both regression parameters and is the most complex scenario in the comparison. This
458 finding is consistent with the results by the $NSE_{\text{sqr}}t$ criterion, and showed the validity
459 of the spatial coherence of both regression parameters in ensuring the robustness of
460 the hydrological projection performance. In addition, when compared DIC results of
461 scenarios 4 and 5, the setting of time-varying functions improved the DIC

462 performance in both DSST schemes. This finding also agreed with the results by the
463 NSE_{sqrt} criterion, and indicated the positive implications by the time-varying model
464 parameters on the projection performance.

465 Tables 6 and 7 illustrate the performance of high and low flows during the
466 verification period in terms of MaxF and MinF estimates for the median projected
467 streamflows in both DSST schemes. As shown in table 7, for the projection of high
468 flow part, scenario 3 exhibits the best performance in all catchments among five
469 scenarios under the scheme of calibrating in the dry period and verifying in the
470 non-dry period. For the projection performance in the other DSST scheme (Table 6),
471 scenario 3 has the best projection performance in high flow part in catchment 225219
472 and is the second best scenario in the other two catchments. It indicates that the
473 incorporation of spatial coherence of both regression parameters β and ω
474 successfully improves the projection performance in the high flow part. As for the
475 projection of the low flow part, the discrepancy between the results of different
476 scenarios and the observed low flows is not obvious. Furthermore, scenario 3 shows
477 the best projected performance in two catchments (405219 and 405264) in the scheme
478 of calibrating in dry period and verifying in non-dry period, and is the best scenario in
479 catchment 405264 in the scheme of calibrating in non-dry period and verifying in dry
480 period. In addition, scenario 3 is the second best option in catchments 225219 and
481 405219 under the scheme of calibrating in non-dry period and verifying in dry period.
482 Combined with the projection performance of both high and low flows, scenario 3

483 achieves its superior projection performance mainly by the improvement in the
484 prediction of high flow parts.

485 Figure 7 shows the BIAS estimates for the median of the posterior distribution of
486 model parameters for all modeling scenarios across all catchments when
487 transferability between the non-dry and dry periods was examined. Although the
488 BIAS was a component of the objective function (Eq. 3), the 10-year rolling average
489 BIAS still deviated considerably from a value of 1 for all the scenarios in the two
490 DSST schemes. The median estimates of the posterior distribution in both scenarios
491 performed well in the NSE_{sqrt} criterion for both periods. However, the median
492 estimates did not ensure unbiased simulations over the modeling period; one scenario
493 with a higher NSE_{sqrt} criterion may have an altered BIAS during the modeling period.
494 The BIAS results in catchments 225219 and 405219 showed some similarity: all
495 scenarios tended to underestimate streamflow along the time sequence in both DSST
496 schemes. Conversely, all scenarios tended to overestimate the streamflow in
497 catchment 405264 in both schemes. By comparing the BIAS performance for the five
498 scenarios, it was observed that the spatial setting of modeling scenarios generally
499 tended to enlarge the BIAS in all catchments, while the difference between scenarios
500 4 and 5 was very small.

501 **4.3 Parameter uncertainty analysis**

502 The uncertainty of the parameters was characterized by the posterior distribution
503 of the regression parameters and was derived by the MCMC iteration. As mentioned

504 in section 2.3.2, regression parameters β and ω were assumed to have different
505 levels of spatial coherence in each modeling scenario (Table 1); these scenarios in
506 each DSST regime are compared in Figs. 8 and 9. It should be mentioned that there
507 was no regression parameter in scenario 5. Solid lines in the violin plots represent the
508 25th and 75th percentiles of the posterior distribution. The dotted line in the violin plot
509 denotes the median estimate of the posterior distribution. In the upper plots in Figures
510 8 and 9, it can be clearly seen that the first three scenarios had a much smaller
511 variation interval than scenario 4 in terms of regression parameter β , which denotes
512 the amplitude of the sine function. The catchment averages of both schemes of the
513 median estimates of β in the first three scenarios are 2.78, -4.91, and 9.26
514 respectively, while that in the fourth scenario is much larger, reached at -39.20.
515 Scenario 3, which considered both spatial coherence of regression parameters β
516 and ω , has the narrowest interval of β for all catchments, followed successively
517 by scenario 1 (only considered the spatial coherence of the regression parameter β),
518 scenario 2 (only parameter ω was spatially coherent), and scenario 4 (no parameter
519 was spatially coherent). With regards to the regression parameter ω , which denotes
520 the frequency of the sine function (in the lower figures of Figures 8 and 9), its median
521 estimates in both four scenarios differ slightly. As shown in Figure 8, the catchment
522 averages of regression parameter ω for different scenarios are 0.24, 0.14, 0.15, and
523 0.18, while those in Figure 9 are 0.15, 0.26, 0.23, and 0.17 respectively. The phase T
524 of the sine term could be derived based on the estimates of ω by equation $T =$
525 $2\pi/\omega$. Thus, the mean phases T of model parameter θ_1 for different scenarios are

526 26.2, 46.3, 41.9 and 35.2 in Figure 8, respectively. Similarly, the mean phases T are
527 42.9, 24.1, 27.4 and 38.0 in Figure 9, respectively.

528 In summary, by combining the results of parameter uncertainty estimation and
529 model projection performance evaluation, the incorporation of spatial coherence
530 successfully improved the robustness of the projection performance in both DSST
531 schemes by controlling the estimation uncertainty of regression parameters β .

532 5. CONCLUSIONS

533 In this study, a two-level HB framework was used to incorporate the spatial
534 coherence of adjacent catchments to improve the hydrological projection performance
535 of sensitive time-varying parameters for a lumped conceptual rainfall-runoff model
536 (GR4J) under contrasting climatic conditions. Firstly, a temporal parameter transfer
537 scheme was implemented, using a DSST procedure in which the available data were
538 divided into non-dry and dry periods. Then, the model was calibrated in the non-dry
539 periods and evaluated in the dry periods, and vice versa. In the first level of the
540 proposed HB framework, the most sensitive parameter in the GR4J model, i.e., the
541 production storage capacity (θ_1), was allowed to vary with time to account for the
542 periodic variation that had significant impacts on the extensionality of the model. The
543 periodic variation in catchment storage capacity was represented by a sine function
544 for θ_1 (parameterized by amplitude and frequency). In the second level, four
545 modeling scenarios with different spatial coherence schemes, and one scenario with a
546 stationary scheme of catchment storage capacity, were used to evaluate the

547 transferability of hydrological models under contrasting climatic conditions. Finally,
548 the proposed method was applied to three spatially adjacent, unregulated, and
549 unimpaired catchments in southeast Australia. The study concludes that: (1) the
550 time-varying setting was valid in improving the model performance but also extended
551 the projection uncertainty in contrast to the stationary setting; (2) the inclusion of
552 spatial coherence successfully reduced the projection uncertainty and improved the
553 robustness of model performance; and (3) a large performance degradation has been
554 found in the DSST scheme with its model parameters calibrated over dry periods and
555 verified in the wet periods. This study improves our understanding of the spatial
556 coherence of time-varying parameters, which will help improve the projection
557 performance under differing climatic conditions. However, there are several unsolved
558 problems that need to be addressed. First, the spatial setting of regression parameters
559 may expand the BIAS between the simulation and streamflow observation with a
560 single objective function; the potential physical mechanism behind this result should
561 be explored further. Secondly, this study was confined to spatially coherent
562 catchments that are similar in climatic and hydrogeological conditions; further
563 research is needed to determine which factors have the most significant impacts on
564 model projection performance when considering obvious inputs from other
565 catchments.

566

567 **ACKNOWLEDGMENTS**

568 This study was supported by the National Key Research and Development
569 Program (2018YFC0407202), the National Natural Science Foundation of China
570 (51861125102; 51879193), the Natural Science Foundation of Hubei Province
571 (2017CFA015), and the Research Council of Norway (FRINATEK Project 274310).
572 The numerical calculations were done on the supercomputing system in the
573 Supercomputing Center of Wuhan University. The authors would like to thank the
574 editor and anonymous reviewers for their comments, which helped improve the
575 quality of the paper.

576 **AUTHOR CONTRIBUTIONS**

577 All of the authors helped to conceive and design the analysis. Zhengke Pan and
578 Pan Liu performed the analysis and wrote the paper. Shida Gao, Jun Xia, Jie Chen and
579 Lei Cheng contributed to the writing of the paper and made comments.

580 **COMPLIANCE WITH ETHICAL STANDARDS**

581 **Conflict of interest:** The authors declare that they have no conflict of interest.

582 **REFERENCES**

583 Ajami, N. K., Duan, Q. Y., and Sorooshian, S.: An integrated hydrologic Bayesian multimodel
584 combination framework: Confronting input, parameter, and model structural uncertainty in
585 hydrologic prediction, *Water Resour. Res.*, 43, 10.1029/2005wr004745, 2007.

586 Bracken, C., Holman, K. D., Rajagopalan, B., and Moradkhani, H.: A Bayesian Hierarchical
587 Approach to Multivariate Nonstationary Hydrologic Frequency Analysis, *Water Resour. Res.*,
588 54, 243-255, 10.1002/2017wr020403, 2018.

589 Brigode, P., Oudin, L., and Perrin, C.: Hydrological model parameter instability: A source of
590 additional uncertainty in estimating the hydrological impacts of climate change?, *J. Hydrol.*,
591 476, 410-425, 10.1016/j.jhydrol.2012.11.012, 2013.

592 Broderick, C., Matthews, T., Wilby, R. L., Bastola, S., and Murphy, C.: Transferability of
593 hydrological models and ensemble averaging methods between contrasting climatic periods,
594 *Water Resour. Res.*, 52, 8343-8373, 10.1002/2016wr018850, 2016.

595 Cha, Y., Park, S. S., Lee, H. W., and Stow, C. A.: A Bayesian hierarchical approach to model
596 seasonal algal variability along an upstream to downstream river gradient, *Water Resour.*
597 *Res.*, 52, 348-357, 10.1002/2015wr017327, 2016.

598 Chen, X., Hao, Z., Devineni, N., and Lall, U.: Climate information based streamflow and
599 rainfall forecasts for Huai River basin using hierarchical Bayesian modeling, *Hydrol. Earth*
600 *Syst. Sci.*, 18, 1539-1548, 10.5194/hess-18-1539-2014, 2014.

601 Chiew, F. H. S., Teng, J., Vaze, J., Post, D. A., Perraud, J. M., Kirono, D. G. C., and Viney, N. R.:
602 Estimating climate change impact on runoff across southeast Australia: Method, results, and
603 implications of the modeling method, *Water Resour. Res.*, 45, 17, 10.1029/2008wr007338,
604 2009.

605 Chiew, F. H. S., Potter, N. J., Vaze, J., Petheram, C., Zhang, L., Teng, J., and Post, D. A.:
606 Observed hydrologic non-stationarity in far south-eastern Australia: implications for
607 modelling and prediction, *Stoch. Environ. Res. Risk Assess.*, 28, 3-15,
608 10.1007/s00477-013-0755-5, 2014.

609 Ciais, P., Reichstein, M., Viovy, N., Granier, A., Ogee, J., Allard, V., Aubinet, M., Buchmann, N.,
610 Bernhofer, C., Carrara, A., Chevallier, F., De Noblet, N., Friend, A. D., Friedlingstein, P.,
611 Grunwald, T., Heinesch, B., Keronen, P., Knohl, A., Krinner, G., Loustau, D., Manca, G.,
612 Matteucci, G., Miglietta, F., Ourcival, J. M., Papale, D., Pilegaard, K., Rambal, S., Seufert, G.,
613 Soussana, J. F., Sanz, M. J., Schulze, E. D., Vesala, T., and Valentini, R.: Europe-wide reduction
614 in primary productivity caused by the heat and drought in 2003, *Nature*, 437, 529-533,
615 10.1038/nature03972, 2005.

616 Clarke, R. T.: Hydrological prediction in a non-stationary world, *Hydrol. Earth Syst. Sci.*, 11,
617 408-414, 10.5194/hess-11-408-2007, 2007.

618 Cook, E. R., Woodhouse, C. A., Eakin, C. M., Meko, D. M., and Stahle, D. W.: Long-term
619 aridity changes in the western United States, *Science*, 306, 1015-1018,
620 10.1126/science.1102586, 2004.

621 Cooley, D., Nychka, D., and Naveau, P.: Bayesian spatial modeling of extreme precipitation
622 return levels, *J. Am. Stat. Assoc.*, 102, 824-840, 10.1198/016214506000000780, 2007.

623 Coron, L., Andreassian, V., Perrin, C., Lerat, J., Vaze, J., Bourqui, M., and Hendrickx, F.: Crash
624 testing hydrological models in contrasted climate conditions: An experiment on 216
625 Australian catchments, *Water Resour. Res.*, 48, 17, 10.1029/2011wr011721, 2012.

626 Deng, C., Liu, P., Guo, S. L., Li, Z. J., and Wang, D. B.: Identification of hydrological model
627 parameter variation using ensemble Kalman filter, *Hydrol. Earth Syst. Sci.*, 20, 4949-4961,
628 10.5194/hess-20-4949-2016, 2016.

629 Deng, C., Liu, P., Wang, D. B., and Wang, W. G.: Temporal variation and scaling of parameters
630 for a monthly hydrologic model, *J. Hydrol.*, 558, 290-300, 10.1016/j.jhydrol.2018.01.049,
631 2018.

632 Duan, Q. Y., Ajami, N. K., Gao, X. G., and Sorooshian, S.: Multi-model ensemble hydrologic
633 prediction using Bayesian model averaging, *Adv. Water Resour.*, 30, 1371-1386,
634 10.1016/j.advwatres.2006.11.014, 2007.

635 Ekstrom, M., Gutmann, E. D., Wilby, R. L., Tye, M. R., and Kirono, D. G. C.: Robustness of
636 hydroclimate metrics for climate change impact research, *Wiley Interdiscip. Rev.-Water*, 5,
637 20, 10.1002/wat2.1288, 2018.

638 Fowler, K. J. A., Peel, M. C., Western, A. W., Zhang, L., and Peterson, T. J.: Simulating runoff
639 under changing climatic conditions: Revisiting an apparent deficiency of conceptual
640 rainfall-runoff models, *Water Resour. Res.*, 52, 1820-1846, 10.1002/2015wr018068, 2016.

641 Gelman, A., Carlin, J., Stern, H., Dunson, D., Vehtari, A., and Rubin, D.: *Bayesian Data Analysis*,
642 third ed ed., CRC Press, 2013.

643 Guo, D. L., Westra, S., and Maier, H. R.: Impact of evapotranspiration process representation
644 on runoff projections from conceptual rainfall-runoff models, *Water Resour. Res.*, 53,
645 435-454, 10.1002/2016wr019627, 2017.

646 Heuvelmans, G., Muys, B., and Feyen, J.: Regionalisation of the parameters of a hydrological
647 model: Comparison of linear regression models with artificial neural nets, *J. Hydrol.*, 319,
648 245-265, 10.1016/j.jhydrol.2005.07.030, 2006.

649 Lebecherel, L., Andreassian, V., and Perrin, C.: On evaluating the robustness of
650 spatial-proximity-based regionalization methods, *J. Hydrol.*, 539, 196-203,
651 10.1016/j.jhydrol.2016.05.031, 2016.

652 Lima, C. H. R., and Lall, U.: Hierarchical Bayesian modeling of multisite daily rainfall
653 occurrence: Rainy season onset, peak, and end, *Water Resour. Res.*, 45, 14,
654 10.1029/2008wr007485, 2009.

655 Lima, C. H. R., Lall, U., Troy, T., and Devineni, N.: A hierarchical Bayesian GEV model for
656 improving local and regional flood quantile estimates, *J. Hydrol.*, 541, 816-823,
657 10.1016/j.jhydrol.2016.07.042, 2016.

658 Liu, P., Li, L. P., Chen, G. J., and Rheinheimer, D. E.: Parameter uncertainty analysis of
659 reservoir operating rules based on implicit stochastic optimization, *J. Hydrol.*, 514, 102-113,
660 10.1016/j.jhydrol.2014.04.012, 2014.

661 Liu, Y. Q., and Gupta, H. V.: Uncertainty in hydrologic modeling: Toward an integrated data
662 assimilation framework, *Water Resour. Res.*, 43, 18, 10.1029/2006wr005756, 2007.

663 Merz, R., and Blöschl, G.: Regionalisation of catchment model parameters, *J. Hydrol.*, 287,
664 95-123, 10.1016/j.jhydrol.2003.09.028, 2004.

665 Merz, R., Parajka, J., and Blöschl, G.: Time stability of catchment model parameters:
666 Implications for climate impact analyses, *Water Resour. Res.*, 47, 17,
667 10.1029/2010wr009505, 2011.

668 Moore, R. D., and Wondzell, S. M.: Physical hydrology and the effects of forest harvesting in
669 the Pacific Northwest: A review, *J. Am. Water Resour. Assoc.*, 41, 763-784, 2005.

670 Moradkhani, H., Hsu, K. L., Gupta, H., and Sorooshian, S.: Uncertainty assessment of
671 hydrologic model states and parameters: Sequential data assimilation using the particle filter,
672 *Water Resour. Res.*, 41, 17, 10.1029/2004wr003604, 2005.

673 Moradkhani, H., DeChant, C. M., and Sorooshian, S.: Evolution of ensemble data assimilation
674 for uncertainty quantification using the particle filter-Markov chain Monte Carlo method,
675 *Water Resour. Res.*, 48, 13, 10.1029/2012wr012144, 2012.

676 Moriasi, D. N., Arnold, J. G., Van Liew, M. W., Bingner, R. L., Harmel, R. D., and Veith, T. L.:
677 Model evaluation guidelines for systematic quantification of accuracy in watershed
678 simulations, *Trans. ASABE*, 50, 885-900, 2007.

679 Najafi, M. R., and Moradkhani, H.: A hierarchical Bayesian approach for the analysis of
680 climate change impact on runoff extremes, *Hydrol. Process.*, 28, 6292-6308,
681 10.1002/hyp.10113, 2014.

682 Nash, J. E., and Sutcliffe, J. V.: River flow forecasting through conceptual models part I — A
683 discussion of principles, *J. Hydrol.*, 10, 282-290,
684 [https://doi.org/10.1016/0022-1694\(70\)90255-6](https://doi.org/10.1016/0022-1694(70)90255-6), 1970.

685 Oudin, L., Andreassian, V., Perrin, C., Michel, C., and Le Moine, N.: Spatial proximity, physical
686 similarity, regression and ungaged catchments: A comparison of regionalization approaches
687 based on 913 French catchments, *Water Resour. Res.*, 44, 15, 10.1029/2007wr006240, 2008.

688 Pathiraja, S., Marshall, L., Sharma, A., and Moradkhani, H.: Detecting non-stationary
689 hydrologic model parameters in a paired catchment system using data assimilation, *Adv.*
690 *Water Resour.*, 94, 103-119, 10.1016/j.advwatres.2016.04.021, 2016.

691 Pathiraja, S., Moradkhani, H., Marshall, L., Sharma, A., and Geenens, G.: Data-Driven Model
692 Uncertainty Estimation in Hydrologic Data Assimilation, *Water Resour. Res.*, 54, 1252-1280,
693 10.1002/2018wr022627, 2018.

694 Patil, S. D., and Stieglitz, M.: Comparing Spatial and temporal transferability of hydrological
695 model parameters, *J. Hydrol.*, 525, 409-417, 10.1016/j.jhydrol.2015.04.003, 2015.

696 Perrin, C., Michel, C., and Andreassian, V.: Improvement of a parsimonious model for
697 streamflow simulation, *J. Hydrol.*, 279, 275-289, 10.1016/s0022-1694(03)00225-7, 2003.

698 Renard, B., Kavetski, D., Leblois, E., Thyer, M., Kuczera, G., and Franks, S. W.: Toward a
699 reliable decomposition of predictive uncertainty in hydrological modeling: Characterizing
700 rainfall errors using conditional simulation, *Water Resour. Res.*, 47, 21,
701 10.1029/2011wr010643, 2011.

702 Saft, M., Western, A. W., Zhang, L., Peel, M. C., and Potter, N. J.: The influence of multiyear
703 drought on the annual rainfall-runoff relationship: An Australian perspective, *Water Resour.*
704 *Res.*, 51, 2444-2463, 10.1002/2014wr015348, 2015.

705 Seiller, G., Anctil, F., and Perrin, C.: Multimodel evaluation of twenty lumped hydrological
706 models under contrasted climate conditions, *Hydrol. Earth Syst. Sci.*, 16, 1171-1189,
707 10.5194/hess-16-1171-2012, 2012.

708 Singh, S. K., Bardossy, A., Gotzinger, J., and Sudheer, K. P.: Effect of spatial resolution on
709 regionalization of hydrological model parameters, *Hydrol. Process.*, 26, 3499-3509,
710 10.1002/hyp.8424, 2012.

711 Spiegelhalter, D. J., Best, N. G., Carlin, B. R., and van der Linde, A.: Bayesian measures of
712 model complexity and fit, *J. R. Stat. Soc. Ser. B-Stat. Methodol.*, 64, 583-616,
713 10.1111/1467-9868.00353, 2002.

714 Sun, X., Thyer, M., Renard, B., and Lang, M.: A general regional frequency analysis
715 framework for quantifying local-scale climate effects: A case study of ENSO effects on
716 Southeast Queensland rainfall, *J. Hydrol.*, 512, 53-68, 10.1016/j.jhydrol.2014.02.025, 2014.

717 Sun, X., and Lall, U.: Spatially coherent trends of annual maximum daily precipitation in the
718 United States, *Geophys. Res. Lett.*, 42, 9781-9789, 10.1002/2015gl066483, 2015.

719 Sun, X., Lall, U., Merz, B., and Dung, N. V.: Hierarchical Bayesian clustering for nonstationary
720 flood frequency analysis: Application to trends of annual maximum flow in Germany, *Water*
721 *Resour. Res.*, 51, 6586-6601, 10.1002/2015wr017117, 2015.

722 Tegegne, G., and Kim, Y. O.: Modelling ungauged catchments using the catchment runoff
723 response similarity, *J. Hydrol.*, 564, 452-466, 10.1016/j.jhydrol.2018.07.042, 2018.

724 Vaze, J., Post, D. A., Chiew, F. H. S., Perraud, J. M., Viney, N. R., and Teng, J.: Climate
725 non-stationarity - Validity of calibrated rainfall-runoff models for use in climate change
726 studies, *J. Hydrol.*, 394, 447-457, 10.1016/j.jhydrol.2010.09.018, 2010.

727 Vrugt, J. A., Gupta, H. V., Bouten, W., and Sorooshian, S.: A Shuffled Complex Evolution
728 Metropolis algorithm for optimization and uncertainty assessment of hydrologic model
729 parameters, *Water Resour. Res.*, 39, 18, 10.1029/2002wr001642, 2003.

730 Vrugt, J. A., ter Braak, C. J. F., Diks, C. G. H., Robinson, B. A., Hyman, J. M., and Higdon, D.:
731 Accelerating Markov Chain Monte Carlo Simulation by Differential Evolution with
732 Self-Adaptive Randomized Subspace Sampling, *International Journal of Nonlinear Sciences
733 and Numerical Simulation*, 10, 273-290, 2009.

734 Westra, S., Thyer, M., Leonard, M., Kavetski, D., and Lambert, M.: A strategy for diagnosing
735 and interpreting hydrological model nonstationarity, *Water Resour. Res.*, 50, 5090-5113,
736 10.1002/2013wr014719, 2014.

737 Wright, D. P., Thyer, M., and Westra, S.: Influential point detection diagnostics in the context
738 of hydrological model calibration, *J. Hydrol.*, 527, 1161-1172, 10.1016/j.jhydrol.2015.05.047,
739 2015.

740 Xiong, M., Liu, P., Cheng, L., Deng, C., Gui, Z., Zhang, X., and Liu, Y.: Identifying time-varying
741 hydrological model parameters to improve simulation efficiency by the ensemble Kalman
742 filter: A joint assimilation of streamflow and actual evapotranspiration, *J. Hydrol.*, 568,
743 758-768, 10.1016/j.jhydrol.2018.11.038, 2019.

744 Xu, Q., Chen, J., Peart, M. R., Ng, C. N., Hau, B. C. H., and Law, W. W. Y.: Exploration of
745 severities of rainfall and runoff extremes in ungauged catchments: A case study of Lai Chi
746 Wo in Hong Kong, China, *Sci. Total Environ.*, 634, 640-649, 10.1016/j.scitotenv.2018.04.024,
747 2018.

748 Yan, H. X., and Moradkhani, H.: A regional Bayesian hierarchical model for flood frequency
749 analysis, *Stoch. Environ. Res. Risk Assess.*, 29, 1019-1036, 10.1007/s00477-014-0975-3,
750 2015.

751 Zhang, X. J., Liu, P., Cheng, L., Liu, Z. J., and Zhao, Y.: A back-fitting algorithm to improve
752 real-time flood forecasting, *J. Hydrol.*, 562, 140-150, 10.1016/j.jhydrol.2018.04.051, 2018.

753 Zhang, Y. Q., Viney, N., Frost, A., and Oke, A.: Collation of Australian modeller's streamflow
754 dataset for 780 unregulated Australian catchments, *Water for a healthy country national
755 research flagship*, 115pp, 2013.

756

757 **TABLES**

758 **Table 1. Different spatial coherence scenarios for regression parameters β and ω in the time-varying functional form of model**
 759 **parameter θ_1 . To explore the performance of spatial coherence within the time-varying function, different levels of spatial coherence for**
 760 **regression parameters β and ω were assumed for the first three scenarios; in contrast, no spatial coherence is assumed in scenario 4, and**
 761 **a temporally stable θ_1 is assumed in scenario 5.**

| Category | Scenario | β | ω | Constraints | |
|----------------|----------------------|---------|---|--|--|
| Time-varying | Spatial coherence | 1 | Parameter β is region-related | Parameter ω is catchment-specific | $\theta_1 = \alpha(c) + \beta(c)\sin[\omega(c)t]$, while $\beta(c) = N(\mu_2, \sigma_2^2)$ |
| | | 2 | Parameter β is catchment-specific | Parameter ω is region-related | $\theta_1 = \alpha(c) + \beta(c)\sin[\omega(c)t]$, while $\omega(c) = N(\mu_3, \sigma_3^2)$ |
| | | 3 | Parameter β is region-related | Parameter ω is region-related | $\theta_1 = \alpha(c) + \beta(c)\sin[\omega(c)t]$, while $\beta(c) = N(\mu_2, \sigma_2^2)$ and $\omega(c) = N(\mu_3, \sigma_3^2)$ |
| Time invariant | No spatial coherence | 4 | Parameter β is catchment-specific | Parameter ω is catchment-specific | $\theta_1 = \alpha(c) + \beta(c)\sin[\omega(c)t]$ |
| | | 5 | No parameters β or ω | | θ_1 is stationary |

762

763 NB: θ_1 represents the production storage capacity of the catchment; β is the slope describing long-term change during the modeling period, and ω is the
 764 amplitude of the sine function describing its seasonal variation during the modeling period; $\mu_2, \sigma_2, \mu_3, \sigma_3$ are hyper-parameters.

765 **Table 2. Comparison of catchments attributes in terms of mean annual rainfall (mm), mean annual evaporation (mm), and mean annual**
 766 **runoff (mm) for 1976–2011.**

767

| Catchments ID | River Name | Observations start | Observations end | Mean annual rainfall | Mean annual potential evapotranspiration | Mean annual runoff |
|---------------|------------|--------------------|------------------|----------------------|--|--------------------|
| 225219 | Macalister | 1/1/1976 | 30/12/2011 | 1064 | 1142 | 350 |
| 405219 | Goulburn | 1/1/1976 | 30/12/2011 | 1169 | 1193 | 422 |
| 405264 | Big | 1/1/1976 | 30/12/2011 | 1406 | 1157 | 469 |

768 **Table 3. Drought identification results for the catchments.**

769

| Catchments ID | Drought start | Drought end | Length | Mean period anomaly | dry % Complete | R ₁ | R ₂ | Change in runoff (%) | Change in rainfall (%) |
|---------------|---------------|-------------|--------|---------------------|----------------|----------------|----------------|----------------------|------------------------|
| 225219 | 1997 | 2009 | 12 | -6.95% | 90.4% | 0.34 | 0.28 | -15.98 | -11.27 |
| 405219 | 1997 | 2009 | 12 | -9.84% | 98.5% | 0.38 | 0.31 | -18.57 | -10.97 |
| 405264 | 1997 | 2009 | 12 | -9.62% | 98.5% | 0.35 | 0.29 | -18.23 | -10.51 |

770 NB: R₁ and R₂ refer to the runoff coefficient during the non-dry and dry periods, respectively.

771

772 **Table 4. Comparison of five scenarios in terms of the deviance information**
 773 **criterion (DIC) when model parameters were calibrated in the non-dry period**
 774 **and verified in the dry period.**

775

| Category | | Scenario | DIC |
|----------------|----------------------|----------|---------|
| | | 1 | 4961.7 |
| Time-varying | Spatial coherence | 2 | 1202.3 |
| | | 3 | -1254.4 |
| | | 4 | 5052.8 |
| | No spatial coherence | | |
| Time invariant | | 5 | 5827.3 |

776

777 **Table 5. Comparison of five scenarios in terms of the deviance information**
 778 **criterion (DIC) when model parameters were calibrated in the dry period and**
 779 **verified in the non-dry period.**

780

| Category | | Scenario | DIC |
|----------------|----------------------|----------|----------|
| | | 1 | -6167.0 |
| Time-varying | Spatial coherence | 2 | -5743.6 |
| | | 3 | -10574.0 |
| | | 4 | -8710.0 |
| | No spatial coherence | | |
| Time invariant | | 5 | -7460.8 |

781

782

783

784

785

786 **Table 6. Comparison of the projection performance of median flows during the**
 787 **verification period associated with the Mean annual maximum flow (MaxF,**
 788 **mm/d) and Mean annual minimum flow (MinF, mm/d) when model parameters**
 789 **were calibrated in the non-dry period and verified in the dry period.**

790

| | Mean annual maximum flow | | | Mean annual minimum flow | | |
|------------|--------------------------|--------------|-------------|--------------------------|--------------|-------------|
| | 225219 | 405219 | 405264 | 225219 | 405219 | 405264 |
| Observed | 10.58 | 11.98 | 9.23 | 0.050 | 0.093 | 0.17 |
| Scenario 1 | 13.30 | 5.64 | 6.68 | 0.050 | 0.045 | 0.13 |
| Scenario 2 | 9.04 | 10.23 | 7.30 | 0.054 | 0.060 | 0.14 |
| Scenario 3 | 10.91 | 7.66 | 9.75 | 0.041 | 0.092 | 0.16 |
| Scenario 4 | 5.91 | 5.42 | 9.54 | 0.089 | 0.089 | 0.15 |
| Scenario 5 | 5.07 | 6.03 | 7.98 | 0.086 | 0.086 | 0.12 |

791 Note:

792 1. The data in 1976 has been used for model warm-up to reduce the impact of the initial soil
 793 moisture conditions during the calibration period, and is not counted in the table;

794 2. The scenarios with bold values are labeled as the best scenario for projecting the
 795 streamflow during the verification periods.

796

797

798

799

800

801

802

803

804 **Table 7. Comparison of the projection performance of median flows during the**
 805 **verification period associated with the Mean annual maximum flow (MaxF,**
 806 **mm/d) and Mean annual minimum flow (MinF, mm/d) when model parameters**
 807 **were calibrated in the dry period and verified in the non-dry period.**

808

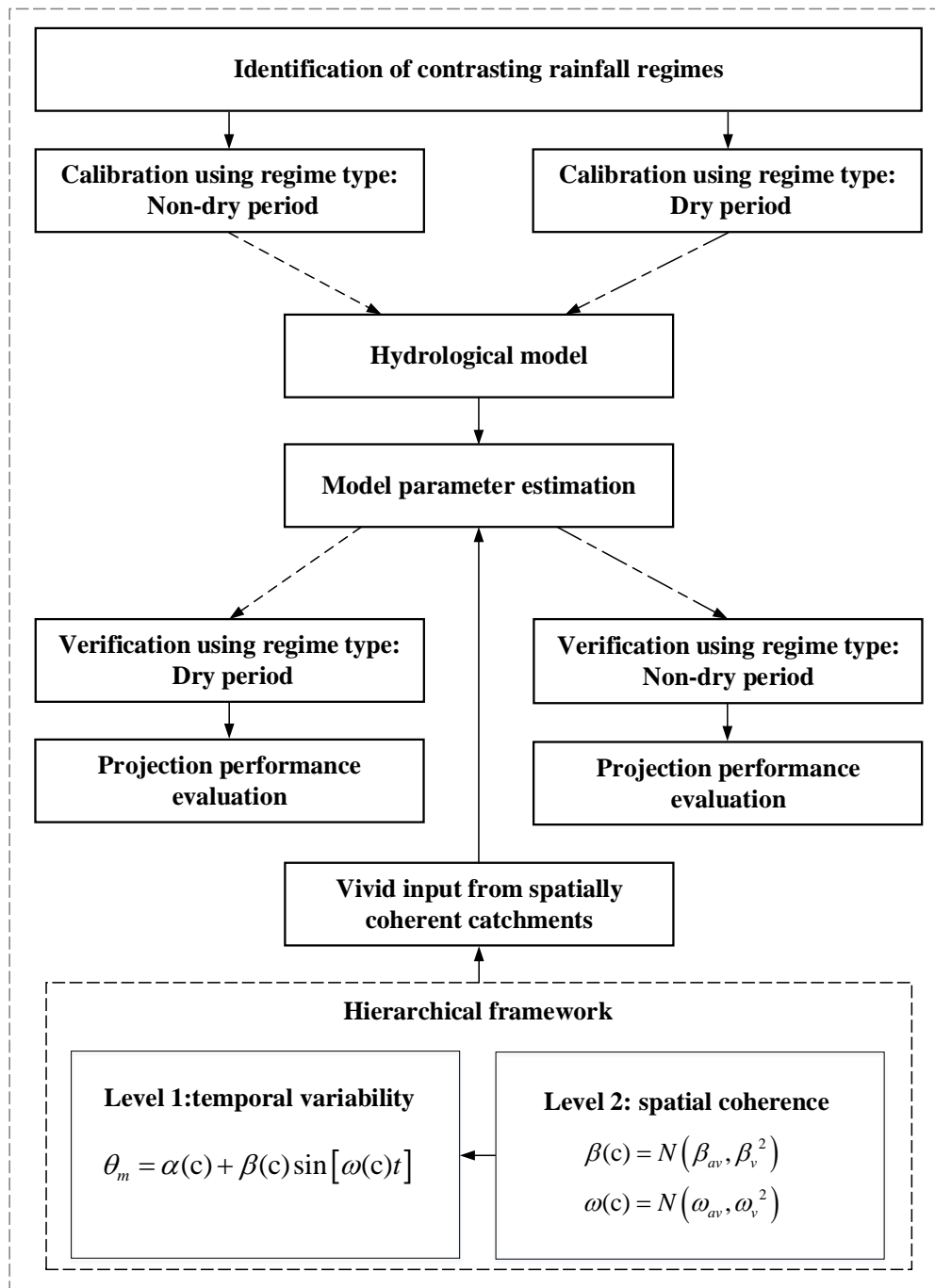
| | Mean annual maximum flow | | | Mean annual minimum flow | | |
|------------|--------------------------|--------------|-------------|--------------------------|-------------|-------------|
| | 225219 | 405219 | 405264 | 225219 | 405219 | 405264 |
| Observed | 10.73 | 12.06 | 8.94 | 0.03 | 0.09 | 0.19 |
| Scenario 1 | 12.40 | 6.87 | 12.90 | 0.03 | 0.04 | 0.09 |
| Scenario 2 | 12.42 | 5.52 | 10.30 | 0.02 | 0.06 | 0.09 |
| Scenario 3 | 10.95 | 10.67 | 8.37 | 0.03 | 0.05 | 0.10 |
| Scenario 4 | 11.98 | 9.85 | 12.34 | 0.03 | 0.05 | 0.10 |
| Scenario 5 | 14.19 | 9.45 | 11.97 | 0.02 | 0.05 | 0.10 |

809 Note:

810 1. The data in 1997 has been used for model warm-up to reduce the impact of the initial soil
 811 moisture conditions during the calibration period, and is not counted in the table;

812 2. The scenarios with bold values are labeled as the best scenario for projecting the
 813 streamflow during the verification periods.

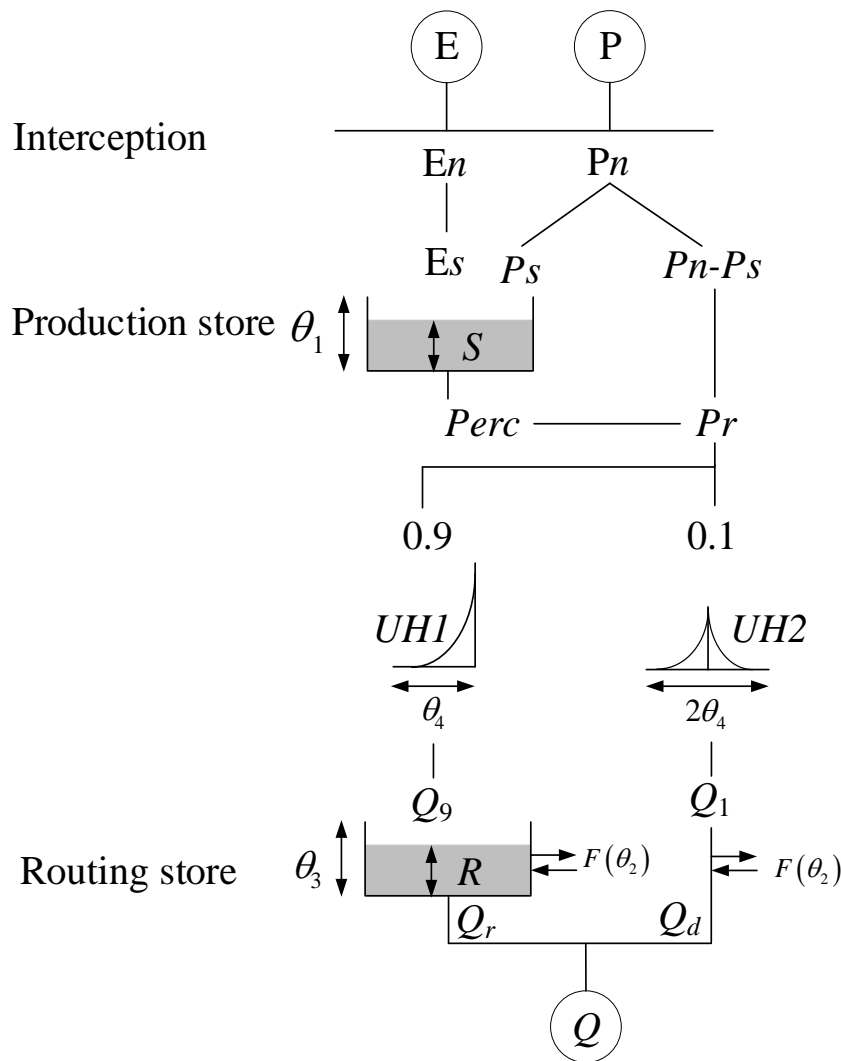
814



816

817 **Figure 1. Flow chart of the methodology for integrating inputs from spatially**
 818 **coherent catchments and temporal variation of model parameters into a**
 819 **hydrological model under contrasting climatic conditions (non-dry and dry**
 820 **periods).**

821

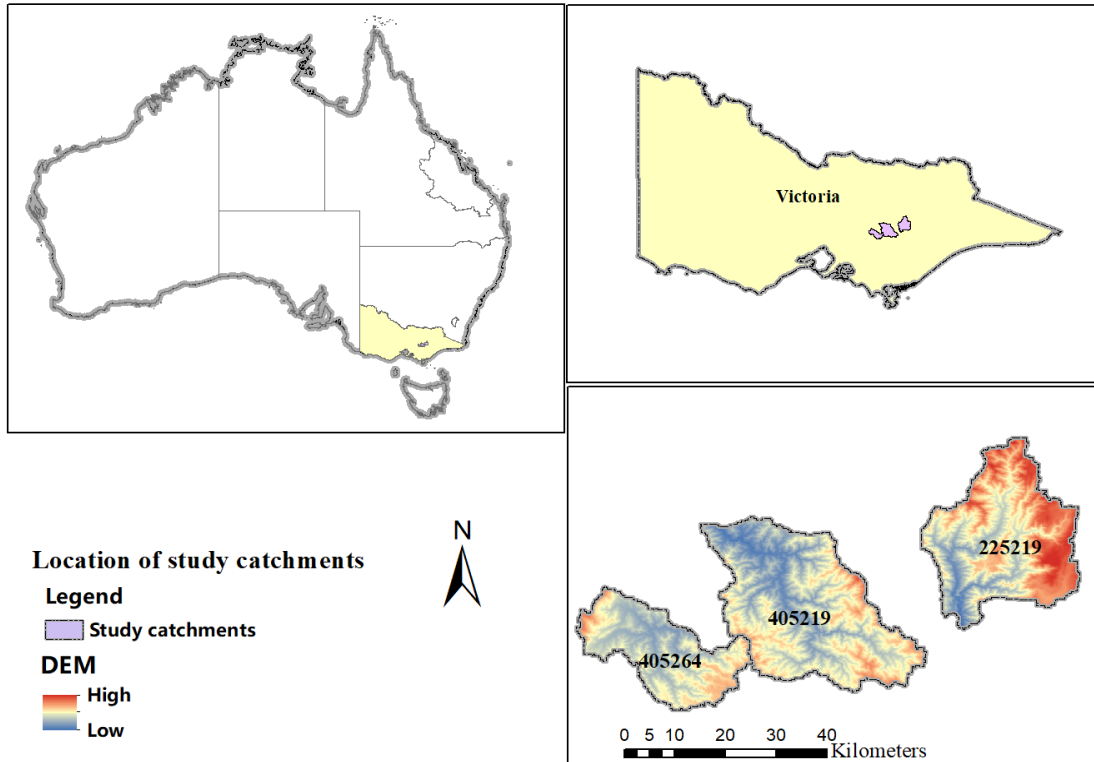


822

823 **Figure 2. Schematic diagram of the GR4J rainfall-runoff model adopted from**
 824 **Perrin et al. (2003). In the figure, P and E refer to precipitation and**
 825 **evapotranspiration, respectively; E_n and P_n denote net precipitation and net**
 826 **evapotranspiration, respectively; P_s refers part of precipitation that fills the**
 827 **production store (i.e. S). The production store is determined as a function of the**
 828 **water level S in production store. The $\theta_1, \theta_2, \theta_3$, and θ_4 denote model parameters.**
 829 **The $Perc$ refers to the percolation leakage that is a function of production store S**
 830 **and parameter θ_1 . The Pr refers to total quantity of water that reaches the**
 831 **routing functions. The $UH1$ and $UH2$ denote two unit hydrographs. The Q_1 and**
 832 **Q_9 refer the corresponding output of the unit hydrographs, respectively; F**
 833 **indicates the groundwater exchange term; R is the level in the routing store. The**
 834 **Q_r refers to the outflow of the routing store, Q_d is a function of water exchange,**
 835 **and Q refers to the total streamflow.**

836

837



838

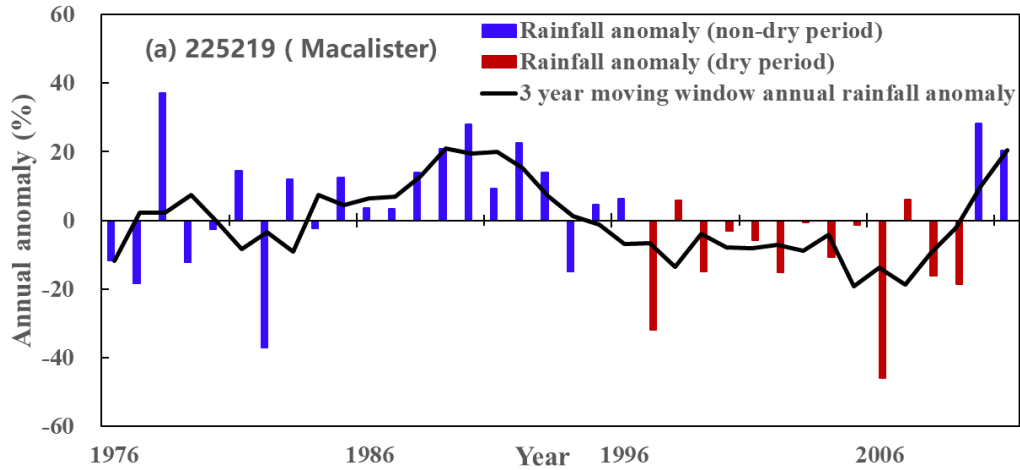
839

840 **Figure 3. Locations of study catchments in Victoria, Australia. The catchment**
 841 **IDs are 225219 (Macalister River catchment), 405219 (Goulburn River**
 842 **catchment), and 405264 (Big River catchment).**

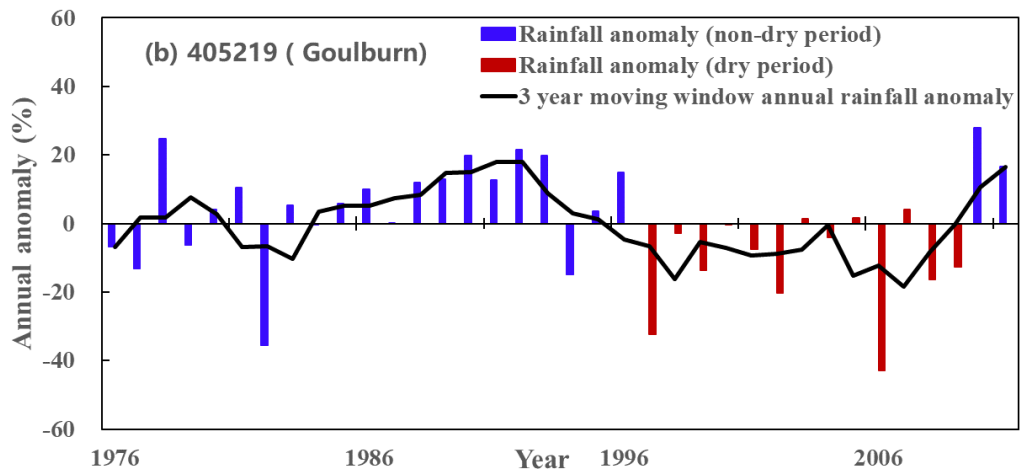
843

844

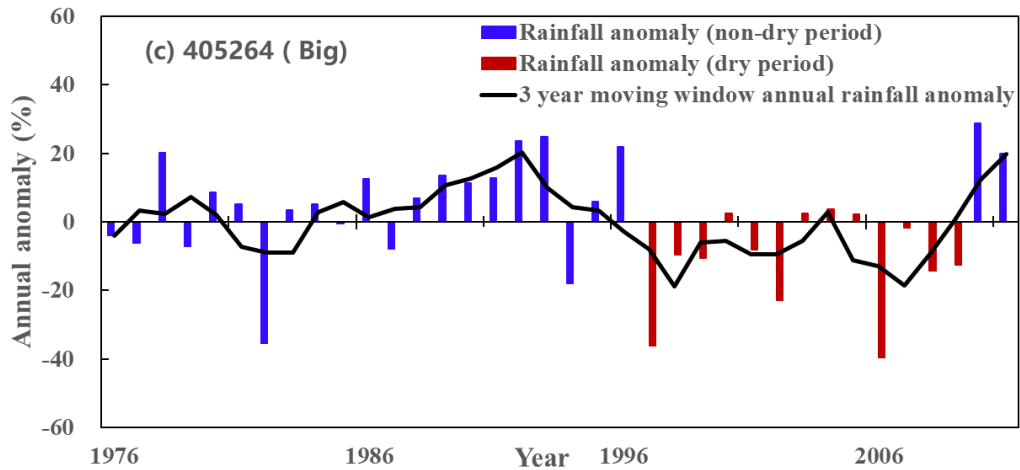
845



846

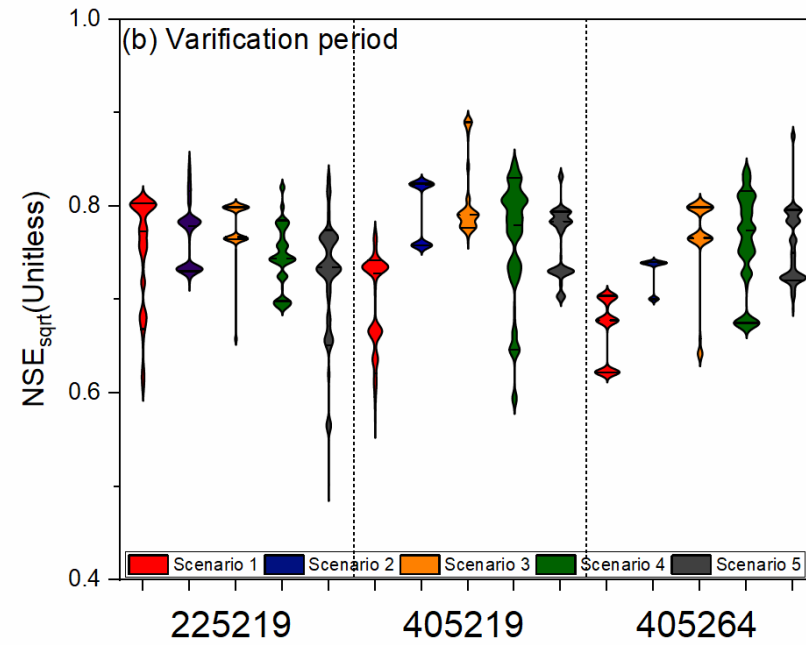
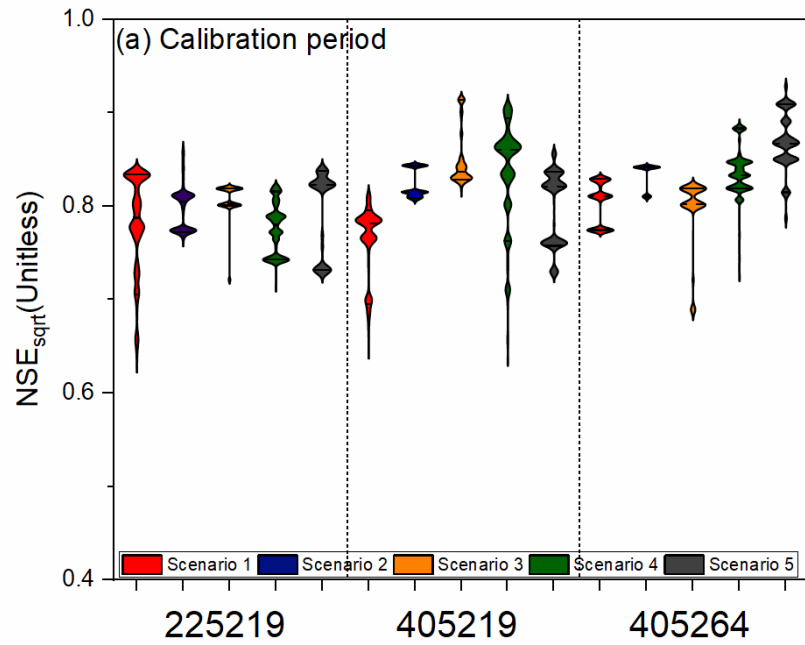


847



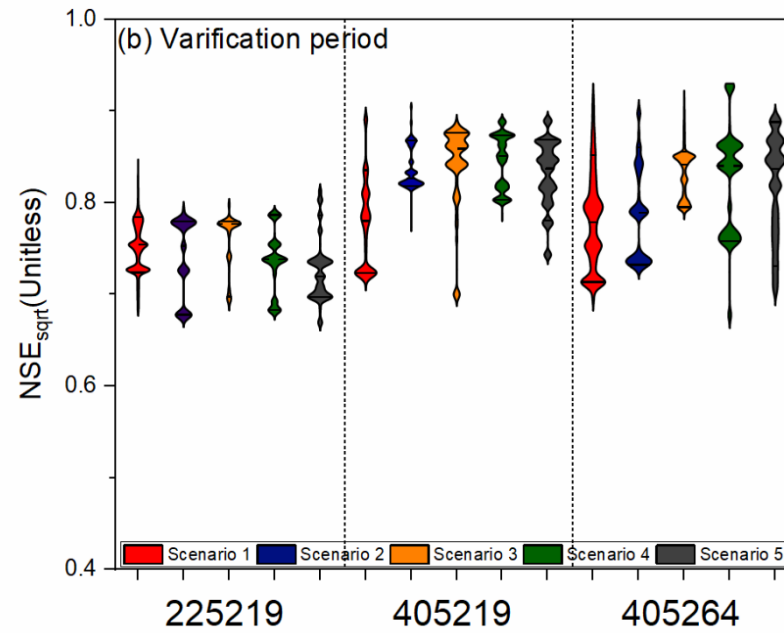
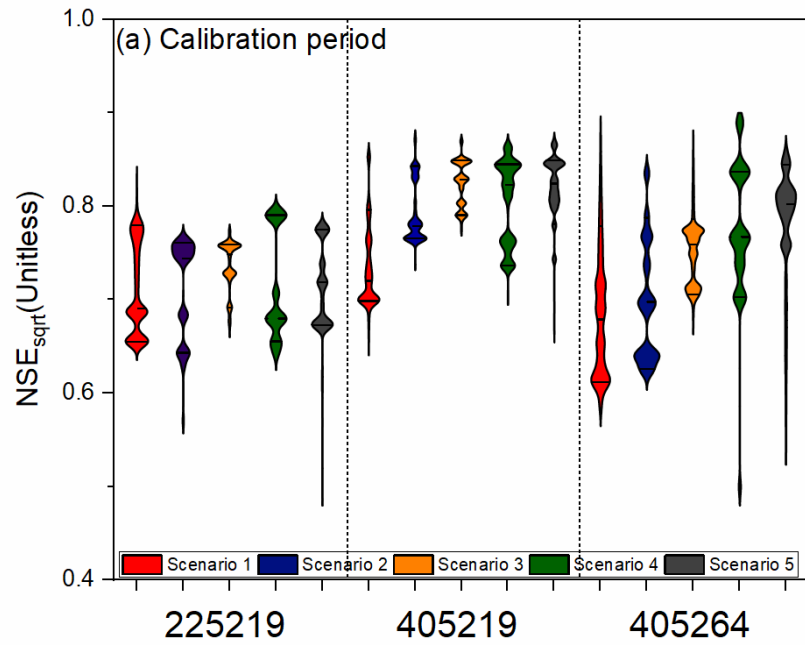
848

849 **Figure 4. The identified dry period in all catchments. The annual anomaly is**
 850 **defined as a percentage of the mean annual rainfall**

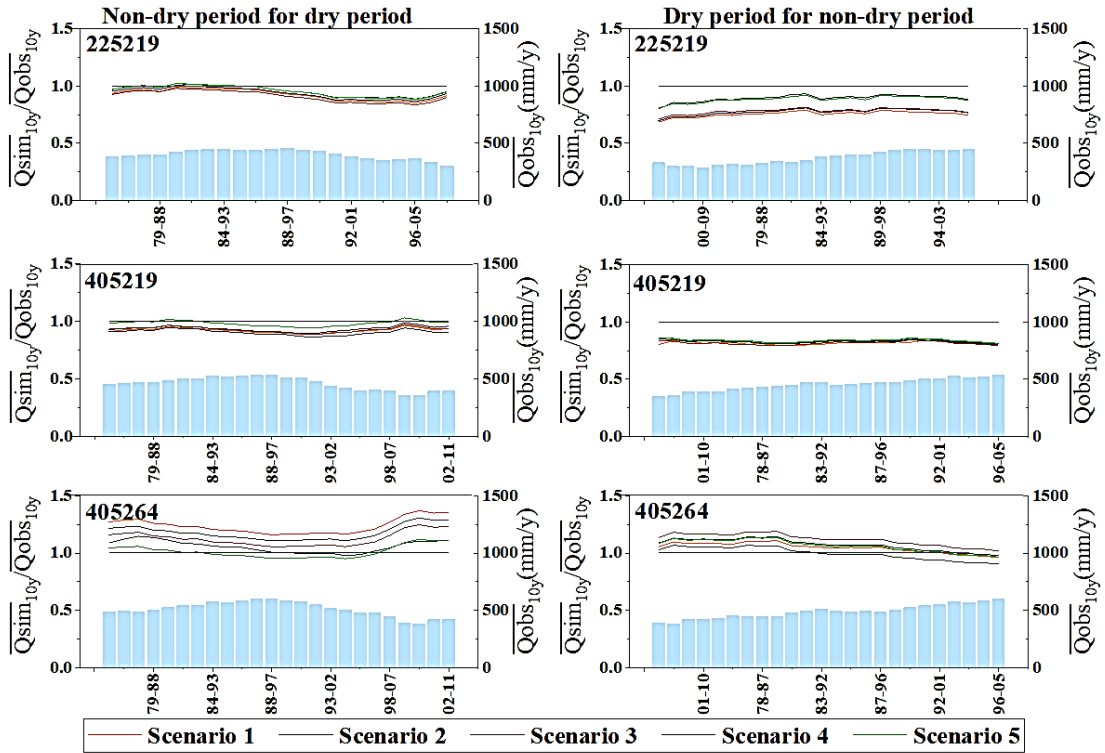


851 **Figure 5. NSE_{sqrt} for each of the five scenarios for each catchment during (a) the calibration period (non-dry period) and (b) the**
 852 **verification period (dry period).**

853



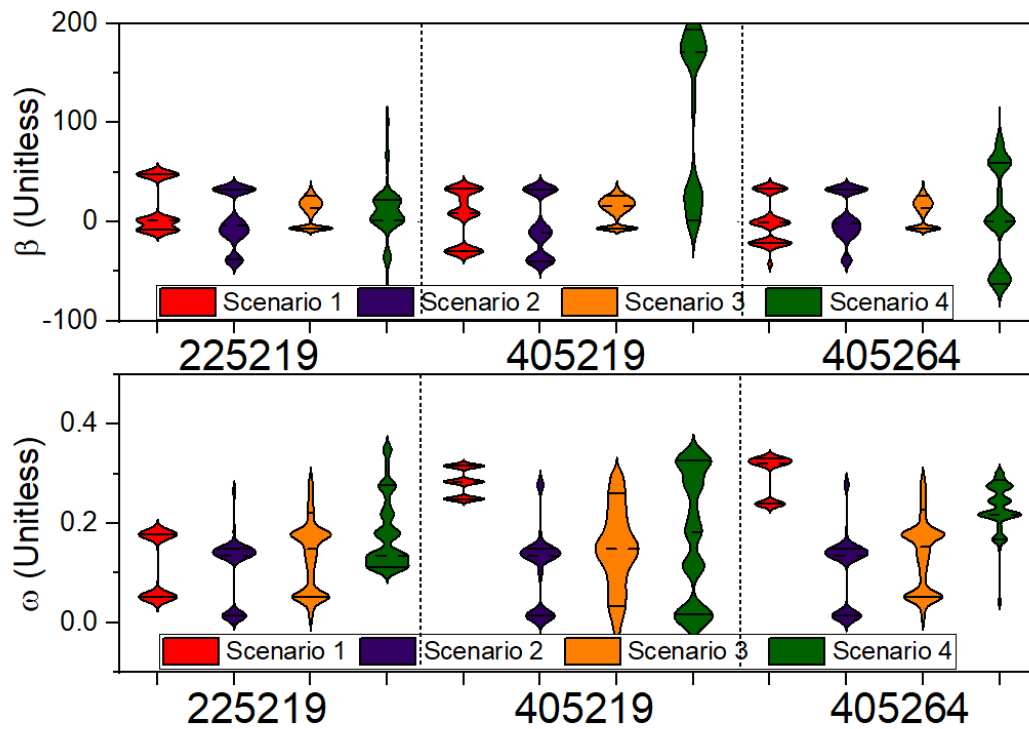
854 **Figure 6. NSE_{sqrt} for each of the five scenarios for each catchment during (a) the calibration period (dry period) and (b) the verification**
 855 **period (non-dry period).**



856

857 **Figure 7. Long-term simulation BIAS of Q_{median} for five scenarios in all**
 858 **catchments. Simulation BIAS is plotted as a 10-year moving average, and**
 859 **10-year moving average streamflows are plotted for reference. The left-hand**
 860 **three graphs are calibrated in the non-dry period and then verified in the dry**
 861 **period, while the opposite sequence applies to the right-hand graphs.**

862

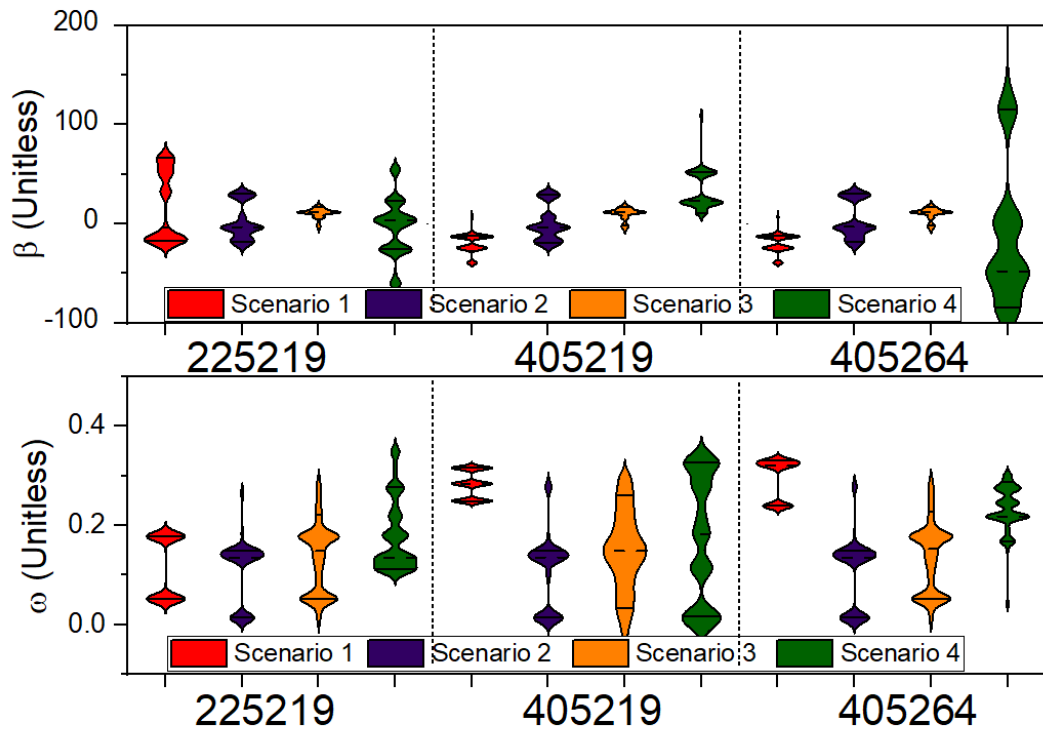


864

865 **Figure 8. Posterior distributions of the regression parameters (β and ω) for the**
 866 **production storage capacity (θ_1) for the four model scenarios in each catchment**
 867 **when calibrated in the non-dry period and verified in the dry period. The solid**
 868 **horizontal lines within the violin plots denote the 25th and 75th percentiles of the**
 869 **posterior distribution, while the dotted line denotes median estimates.**

870

871



872

873 **Figure 9. Posterior distributions of the regression parameters (β and ω) for the**
 874 **production storage capacity (θ_1) for the four model scenarios in each catchment**
 875 **when calibrated in the dry period and verified in the non-dry period. The solid**
 876 **horizontal lines within the violin plots denote the 25th and 75th percentiles of the**
 877 **posterior distribution, while the dotted line denotes median estimates.**